Thermophysical properties of chloropropanes in liquid phase: experiments and simulations

Bernadeta Jasiok, Miroslaw Chorążewski, Alexander Pribylov, Eugene Postnikov, Pascale Friant-Michel, Claude Millot

Journal of Molecular Liquids 358 (2022) 119137

Contents lists available at ScienceDirect

Journal of Molecular Liquids

journal homepage: www.elsevier.com/locate/molliq

Thermophysical properties of chloropropanes in liquid phase: Experiments and simulations

Bernadeta Jasiok [a], Mirosław Chorążewski [a], Alexander A. Pribylov [b], Eugene B. Postnikov [c,*], Pascale Friant-Michel [d], Claude Millot [d,*]

[a] University of Silesia in Katowice, Institute of Chemistry, ul. 9 Szkolna, 40-006 Katowice, Poland
[b] Southwest State University, 50 Let Oktyabrya st., 94, Kursk 305040, Russia
[c] Department of Theoretical Physics, Kursk State University, Radishcheva St., 33, 305000 Kursk, Russia
[d] Université de Lorraine, CNRS, LPCT, F-54000 Nancy, France, Boulevard des Aiguillettes, BP 70239, 54506 Vandoeuvre lès Nancy Cedex, France

ARTICLE INFO

Article history:
Received 11 December 2021
Revised 25 February 2022
Accepted 8 April 2022
Available online 18 April 2022

This work is dedicated to Prof. Gábor Pálinkás on the occasion of his 80th birthday.

Keywords:
Chloropropanes
High-pressures
Thermophysical properties
Span–Wagner EoS
MD simulations
Daridon's method

ABSTRACT

In this work, the properties of liquid 1-chloropropane, 2-chloropropane and 1,3-dichloropropane are investigated. The Span–Wagner equation of state (EoS) is used to improve the existing thermophysical properties as a function of the temperature and pressure of these chloropropanes. For 1-chloropropane and 2-chloropropane, the thermophysical properties are compared with Molecular Dynamics simulation results performed in the range of temperature 293.15–373.15 K and the range of pressure 0.1–200 MPa. In addition, for both monochloropropanes, the isobaric thermal expansion coefficient obtained from Span–Wagner EoS and MD simulations is compared with the one obtained from the recently proposed Daridon's method.

1. Introduction

The interplay of functional forms and parameters of equations of state with macroscopic thermoelastic coefficients and the microscopic molecular nature of the described system is not only of fundamental interest of condensed matter physics and physical chemistry but also is the starting point for most thermodynamic issues related to engineering applications from chemistry and fluid mechanics to materials engineering and nanotechnology. The knowledge of an effective and predictive equation of state and thermoelastic coefficients for a wide range of liquid systems is becoming essential in the context of designing technological processes under high pressure. Therefore, the analysis of the anomalous thermodynamic properties of liquids (thermodynamic response functions) in connection with the molecular structure of liquids acquires an entirely new meaning.

Within this context, a particular interest can be focused on halogenated propanes. They provide an opportunity to explore the influence of the qualitative change of pure *n*-alkane originating from the introduction of the heavy atom. It is possible either symmetrically (with two opposite kinds of effects: in the middle of chain for 2-halogen-propane; and at the end of the molecule for 1,3-halogen-propane) or asymmetrically for 1-halogen-propane. This work focused primarily on one class of chloroalkanes, namely 1-chloropropane, 2-chloropropane, and 1,3-dichloropropane. Experimental datasets are determined in a similar range of thermodynamic conditions intended to validate modeling approaches. In addition, it should be pointed out that haloalkanes have a practical application; namely, they are used, for example, as solvents, propellants, fumigants, disinfectants, or refrigerants [1–4].

However, the prediction of fluid properties over a wide range of thermodynamic states is a complex scientific task. Direct experimental measurement of parameters at high temperature and pressure requires sophisticated equipment. Generally, theoretical

* Corresponding authors at: Department of Theoretical Physics, Kursk State University, Radishcheva St., 33, 305000 Kursk, Russia (E.B. Postnikov), Université de Lorraine, CNRS, LPCT, F-54000 Nancy, France (C. Millot)

E-mail addresses: postnikov@kursksu.ru (E.B. Postnikov), claude.millot@univ-lorraine.fr (C. Millot).

https://doi.org/10.1016/j.molliq.2022.119137
0167-7322/

methods work well for simple systems. Some experimental data are needed to use semi-empirical methods using correlations and approximations. The use of computer simulation methods can generate valuable information and bridge the gap between experiment and theory. This work will apply the Span–Wagner Equation of State (Span–Wagner EoS), known as one of the most accurate empiric correlations that can reproduce the thermodynamic properties in a wide range of temperatures and pressures with an accuracy comparable to the one of practical experimental measurements. Respectively, obtaining parameters of this EoS that allow analytical calculating of primary and derivative thermodynamic quantities gives a background for discussing direct molecular features revealed by MD simulations.

This work will look specifically at the isobaric thermal expansion coefficient $\alpha_P = -\rho^{-1}(\partial\rho/\partial T)_P$, which is known as a thermodynamic quantity quite sensitive to the data and its processing. In particular, the IUPAC recommends paying attention to the reproducibility of α_P's behavior when developing data regression and modeling with equations of state [5]. One of such features of importance is that isotherms of α_P intersect at a given pressure or within a specific range of pressures. In general, they cross below 200 MPa, depending on the temperature range studied [6,7] and the nature of the liquid system [8–10]. In other words, there exist a curve on the thermodynamic plane, where $(\partial\alpha_P/\partial T)_P = 0$. To simplify, we will call this feature as the "intersection of isotherms" instead of the long sentence "zeroing the temperature derivative of the isobaric thermal expansion coefficient".

The experimental data evaluation of three chloropropanes is shown in Section 2. Section 3 is focused on the MD simulations' details. The following section shows how we used experimental data to apply Span–Wagner's method and calculate the fundamental thermodynamic properties from computer simulation results. The discussion section presents the fitting of coefficients and their uncertainty in the Span–Wagner method and different views on calculating the thermal expansion coefficient.

2. Experimental data evaluation

2.1. 1-chloropropane

The experimental data presented in work [11] and other literature sources referenced therein were evaluated using the ThermoData Engine (TDE) [12,13]. It has been revealed that the density data along isotherms $T \geqslant 333.15$ K, i.e., larger than the boiling temperature $T_b = 319.8$ K, and pressures $P \geqslant 10$ MPa looks inconsistent with the rest of the data as it exhibits deviations toward large densities. Thus, these data were rejected, and we need to redetermine the respective values. At the same time, the course of isotherms of the speed of sound satisfies the self-consistent overall picture of the available *PVT* data. Thus, we decided to redetermine the densities based on the modified acoustic route described in details in Lowe et al.'s work [14].

To integrate the thermodynamic equalities

$$\left(\frac{\partial C_P}{\partial P}\right)_T = -\frac{T}{\rho}\left[\alpha_P^2 + \left(\frac{\partial \alpha_P}{\partial T}\right)_P\right], \quad (1)$$

$$\left(\frac{\partial \rho}{\partial P}\right)_T = \left[\frac{T\alpha_P^2}{C_P} - \frac{1}{c^2}\right], \quad (2)$$

where C_P and α_P are the isobaric heat capacity and the coefficient of thermal expansion supplied with the experimental data of the speed of sound, which cubed value is fitted by cubic polynomials along isotherms $c^3(P) = \sum_{n=1}^{2}\sum_{j=0}^{2} A_{jn}(T)(P - P_0)^n$, it is required to state initial conditions along an isobar P_0. Since the temperature interval, $T = (293.15 - 373.15)$ K covers the significant range after the boiling point of 1-chloropropane, the isobar $P_0 = 4.9$ MPa was chosen. Evaluating the data from [11,15] along all these temperature regions and the data from [9] for its part below the boiling point indicates good consistency between these sources. The speed of sound along this isobar was taken from Melent'ev and Postnikov's work [11].

For the isobaric heat capacity, we applied a two-step procedure. The data evaluation demonstrated that the data presented in work [11] need to be slightly shifted by adding a constant value $\Delta C_P = 1.7\text{J}/(\text{mol}\cdot\text{K})$. In this case, the data at 298.15 K are centred concerning the set of available experimental data for this temperature. The whole sequence of C_P values follows a smooth continuous curve formed by the rest of the experimental data and TDE-based predictions for the saturated heat capacity. Note that the shift applied is within the uncertainty range defined for the original data in Melent'ev and Postnikov's work [11]; therefore, this procedure does not out-throw redefined values supplied with the uncertainty range bounded by the original data from the validity range of the experiment. As the next step, the Span–Wagner equation of state for polar substances was fitted to the whole set of available (and not rejected due to large deviations) data using the standard TDE procedure. As a result, the desired heat capacity data for the isobar $P_0 = 4.9$MPa were obtained.

2.2. 2-chloropropane

As done for 1-chloropropane, the recalculation of the density via the acoustic route was carried out. Again, the isobar $P = 4.5$ MPa was chosen as the reference one for the initial conditions; the density ρ_0 and the speed of sound c_0 were taken from the Melent'ev and Postnikov's work [16]. As for the isobaric heat capacity at this pressure, the following procedure was applied. The values at the ambient atmospheric pressure C_P^0 were reported in Melent'ev and Postnikov's work [17]. We used the second-order polynomial interpolation for ρ_0, c_0, and C_P^0 and one step of integration of Eq. (1). As a result, the values of $C_P(4.9\text{MPa})$ for temperatures lower than the boiling point were obtained; in turn, they were interpolated by the second-order polynomial to end the values extrapolated to the temperatures exceeding the boiling temperature. The resulting density at high pressures was found as described above for 1-chloropropane by integrating the system (1) and (2) with the simultaneous uncertainty quantification and applying the processing 10^4 times replicated Monte Carlo ensemble.

2.3. 1,3-dichloropropane

A unique example of halogenated propanes is 1,3-dichloropropane, for which the direct measurements of the isobaric expansion coefficient at high pressures are available [18]. It means that these values can play a role in the reference set since they are not connected to any density approximation method.

At the same time, to the best of our knowledge, despite relatively extensive amounts of saturated data and the data measured at ambient atmospheric pressure [19], the data on the density itself at elevated pressure is absent. However, there exists a dataset of the speed of sound data [20]. Thus, the acoustic route for the density determination, analogous to the one described above, has been carried out. Moreover, the third-order polynomial interpolation was used to determine the isobaric thermal expansion coefficient during the intermediate steps, possibly due to the higher temperature points.

3. Simulation details

MD simulations are performed with home-made simulation codes in periodic boundary conditions (PBC) with N = 1000 rigid molecules in the central cubic box interacting through an atom–atom two-body potential containing Lennard-Jones and Coulomb interactions. The choice of using rigid molecules has been made in order to increase the value of the time step. The molecular geometries have been optimized at Hartree–Fock level with a 6-31G* basis set. In the case of 1-chloropropane, the molecule has three important conformational isomers corresponding to different values of the torsion angle C–C–C–Cl: one trans ($\simeq 180^o$) and two gauche ($\simeq$60° and $\simeq$300°) conformers. In order to approximate the experimental situation as close as possible for each studied thermodynamic state, the experimental percentages of each conformer trans, gauche$^+$, and gauche$^-$ have been used. These populations at different temperatures and pressures have been interpolated from the results of a Raman study [21]. The number of 1-chloropropane conformers and the molecular geometries are given in Tables S1 and S2 of the Supplementary Information, respectively.

Atomic partial charges have been fitted from ab initio calculation at Hartree–Fock level with the 6-31G* basis set in order to reproduce the electrostatic potential around the molecule (ESP charges). Points are located around the molecule with a spacing of 0.35 Å in each Cartesian direction with points located at distances between 1.0 and 2.0 times the van der Waals radius of each atom and removing points closer from any atom than 1.0 times its van der Waals radius. The van der Waals radii are taken from Bondi for the carbon and chlorine atoms and Rowland for the hydrogen atom [22,23]. The grids around the three conformers of trans, gauche$^+$, gauche$^-$ 1-chloropropane, and 2-chloropropane have 6659, 6563, 6563, and 6506 points, respectively. Charges of hydrogen atoms of each CH_2, of each CH_3 groups, and terminal carbon atoms in 2-chloropropane are fitted with a constraint of equality. Then, for 1-chloropropane, an average is taken over the three conformers in order to use a single charge-set. Charges of 1-chloropropane are eventually scaled by 0.99. The ratio of the dipole moment of both isomers of chloropropane would be equal to the value obtained with the ab initio values of the dipole moments. Ab initio calculations have been performed using the Gaussian package [24], and atomic charges are fitted using a home-made code based on the standard minimization of mean-square deviation between the electrostatic potential obtained from the ab initio calculation and the one obtained from the atomic-charge model. The Lennard-Jones parameters have been taken from the OPLS-AA force field, and consistently geometric combination rules are applied for $\epsilon_{a,b}$ and $\sigma_{a,b}$ parameters for pairs of dissimilar atoms a and b [25]. The atomic charges and Lennard-Jones parameters are gathered in Table S3 of the Supplementary Information.

Equations of motion are solved using the center of mass degrees of freedom and a leapfrog quaternion algorithm due to Svanberg [26] with a time step equal to 4 fs. This scheme improves a previous algorithm developed by Fincham [27,28]. In this approach, each molecule's quaternion vector $\mathbf{Q}(t+\Delta t/2)$ is obtained iteratively. In our code, iterations are stopped when the norm of its variation between two consecutive iterations is lower than 10^{-9}. Electrostatic interactions are computed using lattice summations based on the Ladd approach, initially proposed for assemblies of point dipoles [29–31] and generalized to systems of point charges [32,33], leading to expressions equivalent to the ones proposed by other groups [34,35]. A reaction field contribution is added with the dielectric constant of the surrounding continuum equal to infinity, making the method physically equivalent to the standard Ewald approach [31]. It has been observed that the truncation at rank 10 of the expansion of the electrostatic interaction energy in cubic harmonics leads to good accuracy even for highly polar and polarizable systems [31,36]. The van der Waals interactions are truncated beyond a molecular-based cutoff of 20.0 Å. Usual corrections on potential energy and pressure due to this cutoff have been applied [28].

4. Results

4.1. 1-chloropropane

The complete set of the initial data used for solving Eqs. 1,2 is listed in Table 1. The resulting density was found by integrating the (1) and (2) system using the Heun's method with these initial conditions applying the second-order polynomials along isobars for determining the coefficient of thermal expansion and its derivative with respect to pressure. Table S4 in the Supplementary Information presents the obtained values. The standard uncertainty of the data was determined by the Monte Carlo method of uncertainty quantification [37,38]. Each initial condition was replicated 10^4 times to form a Gaussian ensemble with the dispersions corresponding to the values listed in Table 1.

Fig. 1 presents the density values compared to other known data for some of these isotherms. One can see that the behavior of the isotherms for temperatures $T > T_b$ significantly deviates from the values listed in the table of densities in Melent'ev and Posnikov's work [11]. On the contrary, for $T < T_b$, the values of both sets are reasonably consistent, with an average absolute deviation AAD = 0.002. The same is true in a direct comparison with the data from [9] for two isotherms with coinciding temperatures AAD = 0.001, i.e., the correspondence is even better, which is also visible in Fig. 1, where asterisks are practically overlapped with circles. As an additional criterion, isotherms from Bridgman's work [39] are shown. They correspond to the temperatures that do not coincide with those we considered. However, the position, slope, and curvature of these intermediate curves support the accuracy of the new proposed dataset. In particular, when comparing the highest pressure region for the isotherm T = 293.15K and Bridgman's isotherm T = 273.15K, we can conclude that the deviation of crosses (previous data from Ref. [11]) from new (circles) is irrelevant and new (more extensive and less curved) data should be preferred. Finally, it can be pointed out that comparison of the data listed in Table 1 for $P \geqslant 10$ MPa with the prediction of the initial TDE's Span–Wagner model built by fitting the data (except the

Table 1
Thermodynamic parameters at the pressure $P_0 = 4.9$MPa, which play the role of initial conditions for the system 1,2. Their standard uncertainties are $u(\rho) = 2.2\text{kg}\cdot\text{m}^{-3}, u(c) = 3.4\text{m}\cdot\text{s}^{-1}, u(C_P) = 1.8\text{J}\cdot\text{mol}^{-1}\cdot\text{K}^{-1}$.

T/K	293.15	313.15	333.15	353.15	373.15
$\rho(P_0)$/kg · m^{-3}	896.5	871.6	846.3	820.5	794.3
$c(P_0)$/m · s^{-1}	1117.4	1028.3	943.1	862.8	788.0
$C_P(P_0)$/J · mol^{-1} · K^{-1}	128.2	132.5	137.2	142.3	147.9

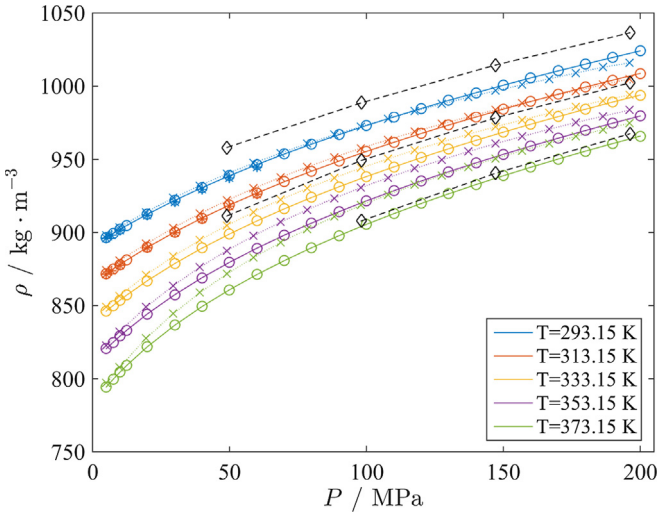

Fig. 1. The density found via the speed of sound-based thermodynamic route (circles), the data from [11] (crosses) for isotherms listed in Table S4 in the Supplementary Information (from up to down). For comparison, the data from [9] for $T = 293.15$K and $T = 313.15$K are shown as asterisks and the data from [39] for $T = 273.15$K, $T = 323.15$K, and $T = 368.15$K as black diamonds. Lines connect markers for visual guidance.

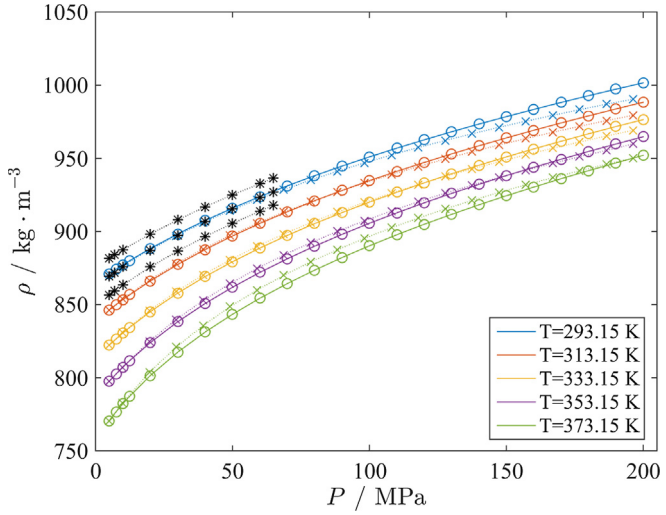

Fig. 2. The density found via the speed of sound-based thermodynamic route (circles), the data from [16] (crosses) for isotherms listed in Table S5 in the Supplementary Information (from up to down). For comparison, the data from [9] for $T = 283.15$K, $T = 293.15$K and $T = 303.15$K are shown as black asterisks. Lines connect markers for visual guidance.

speed of sound) at temperatures not exceeding T_b for such pressures deviates from these new determined densities with AAD = 0.002.

Thus, we can conclude that the dataset for the density of 1-chloropropane published in work [11] should be rejected and replaced with the new dataset given in Table S4.

4.2. 2-chloropropane

Fig. 2 illustrates the pressure dependence of the density obtained via acoustic route presented in Table S5 in the Supplementary Information compared to the data given in Ref. [16] and three isotherms from Ref. [9]. Unfortunately, there is no other data related to this compound at high pressures. One can see that again, newly obtained values are well-coordinated with the previously reported ones for temperatures below the boiling point as it was noted for 1-chloropropane. However, one can see deviations for $P > 100$MPa. Nevertheless, for lower pressures, the correspondence is quite accurate; in particular AAD = 0.1% (1.06kg · m^{-3} in the dimensional form) that is reliably within the experimental uncertainty for the isotherm 293.15K from [9], the only one which coincides with these data in the temperature value. Two other isotherms, which go on both sides from the mentioned one, also demonstrate coordinated position and shape with the newly obtained one. For the two largest temperatures in the studied interval, there is the visible deviation of data from Ref. [16] in the intermediate region of pressures that we can associate with the possible instrumental inaccuracies affecting the results of volumetric density determination in the cited work.

4.3. 1,3-dichloropropane

The obtained results are listed in Table S6 in the Supplementary Information. Unfortunately, to the best of our knowledge, there are no other data for this liquid.

4.4. MD Simulations

1-chloropropane and 2-chloropropane have been studied at six temperatures (293.15, 303.15, 313.15, 333.15, 353.15 and 373.15 K) and densities have been fitted to get eight pressures (0.1, 12,5, 25.0, 50.0, 75.0, 100, 150.0 and 200.0 MPa). In the first stage, the volume is adjusted to get the desired pressure using constant volume simulation with frequent scaling of velocities and angular momenta to impose the desired temperature. Pressure is averaged over 50000–100000 time step periods and used iteratively to guide volume change. When the right density is obtained, the system is simulated at constant energy and volume during a production period of 400000 time steps. The imposed energy is the average total (internal) energy obtained in the last 25000 time steps of the last thermalization run (see Table S8 of the Supplementary Information). Due to finite time step and cutoff of Lennard-Jones interactions, a rescaling of velocities and angular momenta is performed every 500-time step in order to maintain the total energy constant. Among the 48 thermodynamical states of both systems, the root-mean-square deviation between the imposed energies and the MD averaged energies (over 1.6 ns) is around 0.6 J/mol and the maximum deviation is 1.6 J/mol. Averaged translational and rotational temperatures, computed during the simulation from molecular velocities and angular momenta, are very close to the target values. The root-mean-square deviations of the translation and rotational temperatures for the 96 MD runs for the target values is ≃0.3 K. The maximum deviation is 0.75 K. The averaged pressures differ from the target values by less than 1 % for the systems under pressure. At 0.1 MPa, the deviations are within the range ±0.2 MPa.

5. Discussion

5.1. Span–Wagner EoS for chloropropanes: coefficients fitting and uncertainty evaluation

With the datasets prepared in the previous sections supplied additionally with the other available experimental data given in the NIST standard reference database 103b [19], the fitting of polar Span–Wagner EoS for 1-chloropropane, 2-chloropropane, and 1,3-dichloropropane was carried out with the TDE fitting tool by employing the "simulated annealing" fitting procedure.

The Span–Wagner EoS operates with the Helmholtz free energy per unit mass A_m as a thermodynamic potential for obtaining other

thermodynamic properties of the substance, written in the following form:

$$a(\delta,\tau)=\frac{A_m}{RT}=a^0(\delta,\tau)+a^r(\delta,\tau) \tag{3}$$

where $\delta=\rho/\rho_c, \tau=T_c/T$ with ρ_c as the critical density and T_c as the critical temperature, R is the specific gas constant, a^0 is the ideal gas part of the Helmholtz free energy, and a^r is the residual part.

For the polar Span–Wagner EoS, the residual part of Eq. (3) is usually found as the following sum:

$$a^r(\delta,\tau)=\sum_{i=1}^{5}n_i\delta^{d_i}\tau^{t_i}+\sum_{i=6}^{12}n_i\delta^{d_i}\tau^{t_i}e^{-\delta^{c_i}} \tag{4}$$

The ideal gas part of Eq. (3) is usually obtained from the ideal gas heat capacity function $C_P^0(T)$ by calculating the integrals in the following expression:

$$a^0(\delta,\tau)=\frac{1}{RT}\left(\int_{T_0}^{T}C_P^0dT+h_0^0\right)-$$

$$1-\frac{1}{R}\left(\int_{T_0}^{T}\frac{C_P^0-R}{T}dT+R\ln\left(\frac{\rho}{\rho_0^0}\right)+s_0^0\right) \tag{5}$$

where all variables with the lower index "0" refer to an arbitrary reference state and do not contribute to the derived liquid's properties, the $C_P^0(T)$ functions for all studied substances are provided by TDE as a 4-degree polynomial $C_P^0(T)/R=\sum_{i=0}^{4}C_iT^i$. Thus, the integration of Eq. (5) gives the following form of $a^0(\delta,\tau)$ for this type of the $C_P^0(T)$ fitting function:

$$a^0(\delta,\tau)=\ln\delta+a_0\ln\tau+a_1\tau^{-1}+a_2\tau^{-2}+a_3\tau^{-3}+a_4\tau^{-4} \tag{6}$$

For 1-chloropropane, the following constants were used for fitting: $T_c=503.305$ K, $\rho_c=3.733$ mol/l and $R=105.862$ J/kg K. The coefficients, obtained for the ideal gas part in the form of Eq. (6), are the following: $a_0=4.21713431, a_1=0.93881713, a_2=-4.95589391, a_3=2.04005711$ and $a_4=-0.32740601$.

For 2-chloropropane, the following constants were used for fitting: $T_c=482.401$ K, $\rho_c=4.079$ mol/l and $R=105.862$ J/kg K. The coefficients, obtained for the ideal gas part in the form of Eq. (6), are the following: $a_0=5.10191966, a_1=2.65807121, a_2=-5.88923338, a_3=2.47291938$ and $a_4=-0.41940059$.

For 1,3-dichloropropane, the following constants were used for fitting: $T_c=614.600$ K, $\rho_c=3.473$ mol/l and $R=73.589$ J/kg K. The coefficients, obtained for the ideal gas part in the form of Eq. (6), are the following: $a_0=6.76492505, a_1=3.25768226, a_2=-8.92941215, a_3=4.54996311$ and $a_4=-0.91194098$.

The coefficients of Eq. (4), obtained from the fitting procedure, are listed in Table S7 (note that coefficients d_i, t_i, and c_i are specific for the polar type of the Span–Wagner EoS and do not vary from one substance to another).

To evaluate the uncertainties of all obtained EoS, the experimental data for density and the speed of sound for compressed and saturated liquid, the heat capacity at constant pressure and the heat capacity at saturation pressure, were used. All data were taken from the TDE database [19], except for the points rejected after performing the Data Evaluation procedure or replaced to the corrected values in the previous sections. The theoretical predictions of the density values at particular pressure and temperature were made by choosing the ρ value that predicts the closest value of pressure by the formula $p(\delta,\tau)=\rho RT(1+\delta a_\delta^r)$, with a ρ increment of $10^{-6}\rho_c$. The equations for the heat capacity per unit mass at constant pressure, heat capacity per unit mass at saturation pressure, and the speed of sound via derivatives of the Helmholtz free energy are following:

$$\frac{C_P(\delta,\tau)}{R}=-\tau^2(a_{\tau\tau}^0+a_{\tau\tau}^r)+\frac{(1+\delta a_\delta^r-\delta\tau a_{\delta\tau}^r)^2}{1+2\delta a_\delta^r+\delta^2a_{\delta\delta}^r} \tag{7}$$

$$\frac{C_s(\delta,\tau)}{R}=-\tau^2(a_{\tau\tau}^0+a_{\tau\tau}^r)+\frac{(1+\delta a_\delta^r-\delta\tau a_{\delta\tau}^r)^2}{1+2\delta a_\delta^r+\delta^2a_{\delta\delta}^r}$$

$$\left[(1+\delta a_\delta^r-\delta\tau a_{\delta\tau}^r)-\frac{\rho_c}{R\delta}\frac{dp_s}{dT}\right] \tag{8}$$

$$\frac{c^2(\delta,\tau)}{RT}=1+2\delta a_\delta^r+\delta^2a_{\delta\delta}^r-\frac{(1+\delta a_\delta^r-\delta\tau a_{\delta\tau}^r)^2}{\tau^2(a_{\tau\tau}^0+a_{\tau\tau}^r)} \tag{9}$$

with $p_s(T)$ as the phase boundary pressure function. In equations above, subscripts δ and τ denote partial derivatives respectively to these reduced variables. To evaluate the uncertainties at the saturation curve, the experimental phase boundary pressure data provided by the TDE database were fitted by the Wagner vapor pressure equation. Using this equation, the values of boundary pressure were added to each data point so that it would be possible to apply the Span–Wagner EoS for calculations. The deviations of the density values, calculated by obtained EoS', from respective experimental values at elevated pressure for all studied liquids are shown in Fig. S1 of the Supplementary Information. The deviations of predicted density values at the saturation curves from the experimental ones are shown in Fig. S2 of the Supplementary Information.

AAD calculation was made for all above-counted quantities in the range of temperatures from 273.15 K to 373.15 K, and for all values of the temperatures presented in considered datasets. Table S10 of the Supplementary Information summarizes the AAD values obtained for all considered substances in compressed liquid and saturated liquid states.

5.2. The isobaric thermal expansion intersection curves and the thermodynamic curvature isolines

Using the Span–Wagner EoS with the obtained coefficients, the isobaric thermal expansion intersection curve and the thermodynamic Riemannian curvature contours were plotted for all studied liquids by the procedure described in the Supplementary Information of Pribylov and Postnikov's work [40]. Fig. S3 of the Supplementary Information shows the obtained isolines of the Riemannian curvature R and the α_P intersection curve on the (P,T) plane, as well as the contours of dimensionless thermodynamic curvature $R^*=R/V_{vdW}$, where V_{vdW} is the van der Waals molecular volume characterizing the size of molecules in (ρ^*,T) coordinates, where $\rho^*=\rho/\rho_{vdW}$ with $\rho_{vdW}=M/N_aV_{vdW}$ as the van der Waals density, where M – molar mass and N_A – Avogadro constant.

One can see that the intersection curve behaves for these liquids in the manner typical of *n*-alkanes, it coincides with an isoline of the thermodynamic curvature when the liquid tends to melt. Around the melting point, such a coincidence is observed for substances with longer chains starting from *n*-pentane rather than for *n*-propane, characterized by the specificity of packing near the melting point [40]. However, this observation is in line with the analysis of the cohesive energy density [41], which indicates that for 1-haloalkanes, introducing chlorine atom (which is significantly heavier than the replaced hydrogen) is equivalent form the point of view of the energy of intermolecular interactions to the ascending shift along with pure alkane's homologous series on just about three members of it, see [42].

Thus, the α_P intersection curves for 1-chloropropane, 2-chloropropane and 1,3-dichloropropane obtained in the present study can be compared to each other and to the one of *n*-propane reported in Pribylov and Postnikov's work [40], by plotting in both dimensionless (ρ^*, T^*) with $T^* = T/T_c$, and (P, T) sets of coordinates. Fig. S4 of the Supplementary Information shows those intersection curves in chosen coordinates. One can see that despite the different position of the intersection curves on the (P, T), three out of four of them are almost merged practically in one narrow stripe on the (ρ^*, T^*) plane. As discussed in [40], this stripe can be interpreted as the universality of molecular packing properties corresponding to the thermodynamic state, where $(\partial\alpha_P/\partial T)_P = 0$. This is also related to the reasons mentioned above that the chlorine atom replacing the hydrogen in the methyl group is equivalent, to the certain extent, to a simple elongation of the alkane's chain. On the contrary, introducing chlorine into the middle methylene group results in the some displacement of the $(\partial\alpha_P/\partial T)_P = 0$ line at low reduced temperatures and its more linear character.

5.3. Comparison of the isobaric thermal expansions obtained in different ways

To compare α_P for two isotherms whose temperatures coincide in the direct measurements [18] and for the acoustic route based on the speed of sound data [20], the acoustic route of the density determination was applied to determine the isobaric thermal expansion coefficient at the same values of pressure that in Chorążewski et al. [18]. Since this interval of pressures overcomes available data in Yebra *et al.* [20], the second-order polynomial extrapolation of the cubed speed of sound was used for $P > 95$MPa and the same order of polynomial was used in the extrapolated region for partial derivatives with respect to the temperature. The Span–Wagner EoS obtained in the previous section also allows to calculate α_P by the following formula:

$$\alpha_P = -\frac{\delta\tau}{T_c}\frac{\tau(a^0_{\delta\tau} + a^r_{\delta\tau}) - a^0_\delta - a^r_\delta}{1 + 2\delta a^r_\delta + \delta^2 a^r_{\delta\delta}}. \tag{10}$$

In this way, it is possible to compare the values of α_P, obtained by these three different methods at the values of the temperature of 303.15 K and 323.15 K (these values are only common for both sources [18,20], the latter was used to obtain α_P through the acoustic route), and the values of pressure, where the experimental measurements were made. The uncertainties of calculations were estimated for each point by the Monte Carlo method for the acoustic route calculations, and by the TDE's EoS calculation instrument for the Span–Wagner EoS calculations. The comparison of the experimental and calculated values of α_P is provided in Fig. S5 of the Supplementary Information.

A comparison of the results of α_P calculations using the previously described acoustic route method and the Span–Wagner EoS can also be done in a wider range of temperatures, where the experimental measurements of the speed of sound in [20] are made. To avoid using extrapolation, the comparison is made only in the interval of pressures, where the values of the speed of sound were measured. Fig. S6 of the Supplementary Information shows the result of calculations of the α_P values with the acoustic route method and the Span–Wagner EoS, carried out at the points where the speed of sound was measured.

Finally, we look at a recently published numerical method, where a limited number of experimental data were used to estimate the isobaric thermal expansion coefficient and its uncertainty [43]. It is based on a proper power-law transformation of variables (density and temperature) that linearizes the experimental points in such a representation. In comparison with the other method where a proper polynomial degree is needed, it is unnecessary here. For the calculations, we used the MD results. To calculate the isobaric thermal expansion coefficient, we used the following equation proposed by Daridon et al. [43]:

$$\alpha_P = -\frac{T_m}{mnT}\frac{a_1}{\rho_n} \tag{11}$$

where T_m and ρ_n are the temperature and density re-expressed as a power transformation $\left(T_m = T^{1/m}; \rho_n = \left(\frac{\rho}{1000}\right)^n\right)$, T is the temperature, and a_1 is the slope of the expression $\rho_n(T_m)$.

The results of MD simulations, carried out for 1-chloropropane and 2-chloropropane, also allow to calculate α_P by making a polynomial interpolation of the obtained values of density from the thermodynamic definition $\alpha_P = \left(-\frac{1}{\rho}\right)\left(\frac{\partial\rho}{\partial T}\right)_P$, with the temperature dependence of the density fitted using a polynomial of order 2. Thus, the comparison of the MD results, the ones predicted by fitting on the experimental data Span–Wagner EoS, and the ones predicted by the Daridon et al. method can be provided. The respective values of α_P for 1- and 2-chloropropane were calculated from the results of the MD simulations by the Span–Wagner EoS' and Daridon *et al.* method at the points where the simulations were made are shown in Fig. 3.

Using the polynomial interpolation of the obtained MD values of density compared to the Daridon et al. method [43], we obtained very similar results in the high-pressure region. Here, the crossing occurs around 150 MPa and in the range of pressures 150–200 MPa for 1-chloropropane and 2-chloropropane, respectively. There is a difference between polynomial and Daridon *et al.* method for the highest temperatures at small pressures. Such behavior is understandable because it corresponds to the state far after the boiling point. The results obtained by the Span–Wagner method differ from those previously mentioned. Here, the crossing occurs in the range 100–122 MPa and 75–115 MPa for two isomers of chloropropane. The intersection ranges occur in relatively close ranges for 1-chloropropane. However, a significant intersection shift is seen for 2-chloropropane. This may be due to obtaining a more significant discrepancy in the MD density results compared to the data obtained with Span–Wagner EoS.

5.4. The other thermodynamic quantities calculated from the MD results

The computer simulations were used to obtain the thermophysical properties for 1-chloropropane, and 2-chloropropane, such as the density, the isothermal compressibility, constant volume and constant pressure heat capacities, and the speed of sound.

The density was calculated using the formula $\rho = \frac{N}{V}$, where N is the number of molecules, and V is the volume. The isothermal compressibility, κ_T, was computed from the thermodynamic definition $\kappa_T = \left(\frac{1}{\rho}\right)\left(\frac{\partial\rho}{\partial P}\right)_T$ with the density dependence of density modeled by the functional form used in the Tait equation.

The constant volume heat capacity was obtained from the fluctuation formula in the *NVE* ensemble [44,45,28]:

$$C_V = \frac{3Nk_B}{1 - \frac{<\delta E^2_{kin}>}{3Nk_B^2T^2}} \tag{12}$$

where $\delta E_{kin} = E_{kin} - < E_{kin} >$, with E_{kin} the total (translational and rotational) kinetic energy of the system of N rigid molecules, k_B being the Boltzmann constant and T is the temperature. The constant pressure heat capacity is computed from the formula $C_P = \left(\frac{\partial H}{\partial T}\right)_P$ where the temperature dependence of the enthalpy H is fitted using a polynomial of order 2. Quantum corrections due to vibrational degrees of freedom for heat capacities are computed

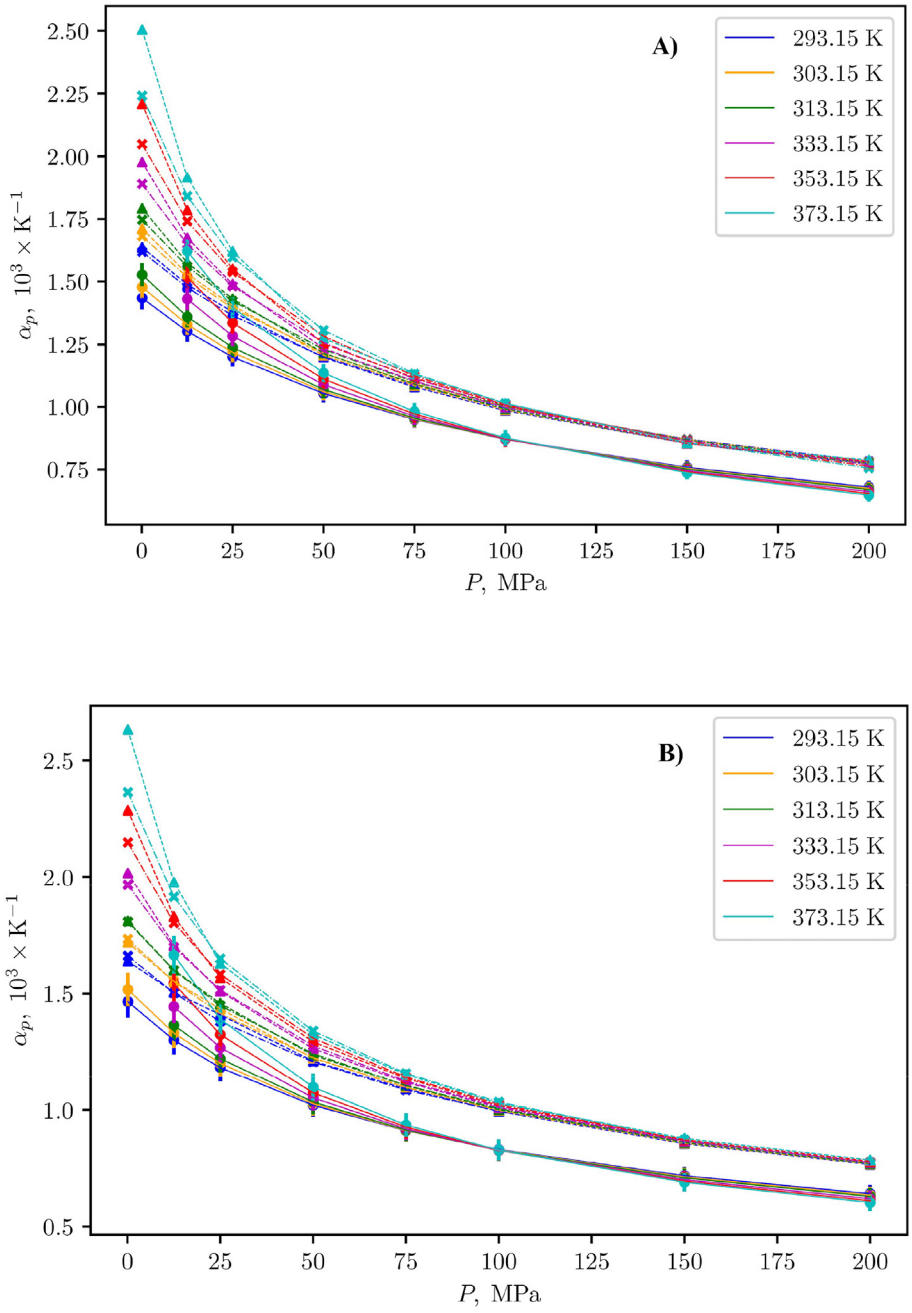

Fig. 3. The isobaric thermal expansion coefficients of 1-chloropropane (A) and 2-chloropropane (B), found from the MD simulations data (crosses), by the obtained Span–Wagner EoS (circles) and the Daridon *et al.* method (triangles) at the points where the simulations were made. Lines connect markers for visual guidance.

assuming a harmonic oscillator model for the molecular vibrations. Values of the vibrational frequencies are taken from the literature. For 1-chloropropane gauche and trans rotamers they are taken from an infrared (IR) study in gas phase; the missing values for the trans rotamer being estimated from the corresponding modes of the gauche conformer and ab initio values from $\nu_{estimatedIR,trans} = \frac{\nu_{IR,gauche} \cdot \nu_{abinitio,trans}}{\nu_{abinitio,gauche}}$ [46]. For 2-chloropropane, observed frequencies from the gas phase and liquid phase IR data are used [47]. Using vibrationally quantum corrected heat capacities, the speed of sound is obtained from the equation:

$$c = \sqrt{\frac{C_P}{C_V} \frac{V}{M\kappa_T}} \tag{13}$$

where M is the mass of the system, the numerical values of the density are given in Table S9 of the Supplementary Information.

The comparison of the thermodynamic quantities obtained from the MD simulations to the respective Span–Wagner EoS is provided in Fig. 4 for 1-chloropropane and Fig. 5 for 2-chloropropane, respectively. The colors of markers and lines match the same temperature values as in Fig. 3.

First, we look at the density (Fig. 4(A)) and Fig. 5(A)). As seen, better results for 1-chloropropane compared to 2-chloropropane were obtained. This is due to a smaller error for 1-chloropropane than 2-chloropropane, for which the density plot is more "elongated". This also explains the behavior of the thermal expansion coefficient discussed above. On the other hand, for both heat capacities, the "almost" monotonic functions from MD results

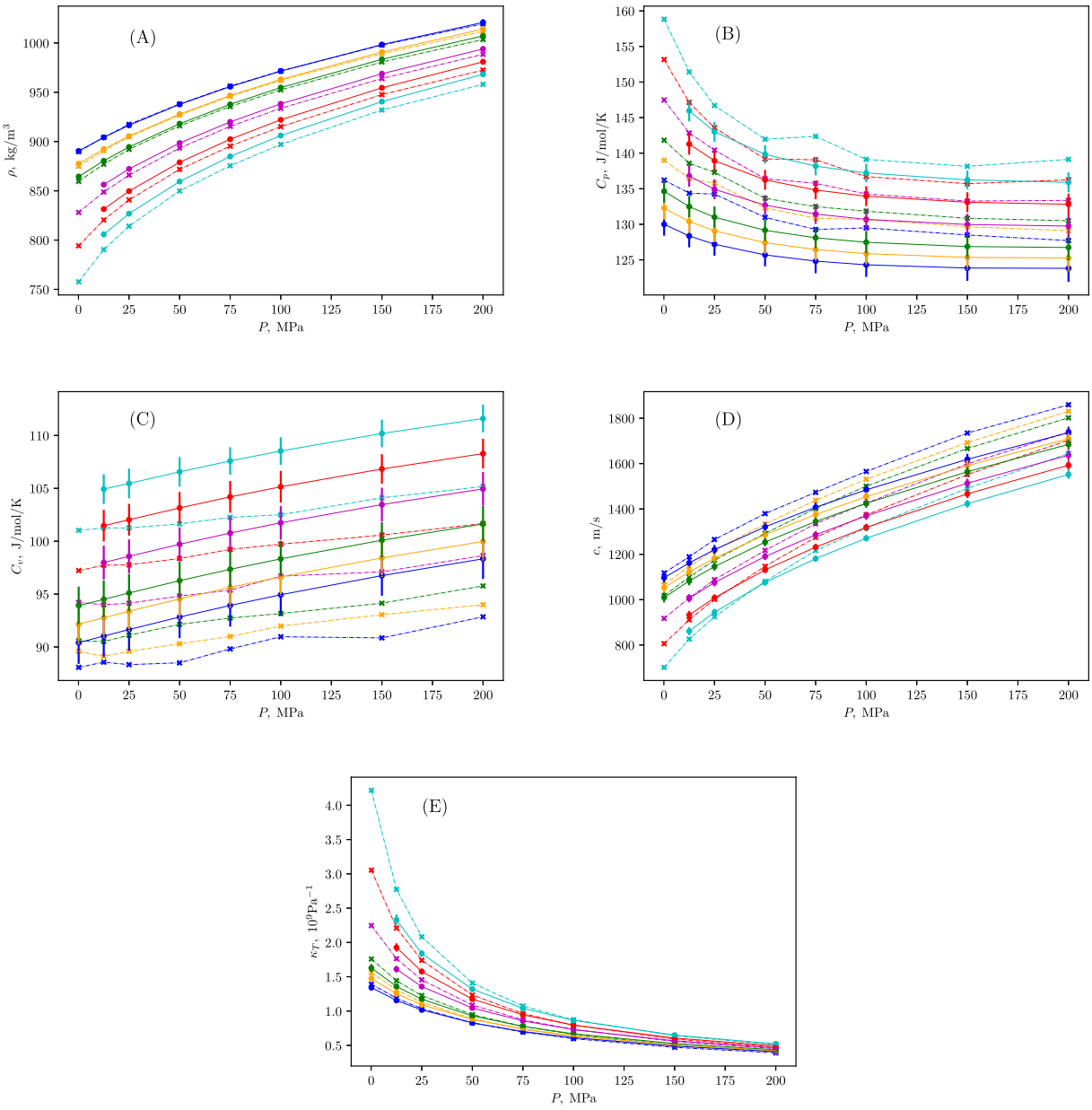

Fig. 4. The comparison of the values of density (A), heat capacity at constant pressure (B), heat capacity at constant volume (C), speed of sound (D) and isothermal compressibility (E) of 1-chloropropane, found from the MD Simulations data (crosses) and by the obtained Span–Wagner EoS (circles) at the points where the simulations were made. Lines connect markers for visual guidance.

(Figs. 4(B), (C)) and Figs. 5(B), (C)) were obtained. This may be due to the use of a small number of energy isotherms used to calculate the constant pressure and constant volume heat capacities. As the temperature increases, the error increases for C_P, while for C_v for each isotherm, the error remains approximately constant. The speed of sound calculated from Eq. 13 is shown in Fig. 4(D) and Fig. 5(D). Here also, we obtained better results for 1-chloropropane, which may be due to the use of the values with error used to calculate the speed of sound from the thermodynamic equation. The Fig. 4(E) and Fig. 5(E) show the results for isothermal compressibility.

For both chloropropanes, we obtain acceptable results except for the results for $P = 0.1$ MPa. Several temperatures are larger than the boiling temperature in these points, which explains the larger deviations. In Table 2 the Absolute Average Deviations (AADs) for each thermodynamic properties of two chlorinated propanes are shown.

One may wonder why simulation results differ between liquids composed of isomers that do not differ significantly. The OPLS force field and ESP/HF-6-31G* charges give a very similar density for both liquids in a given thermodynamic state. In contrast, experimentally, 2-chloropropane has a density lower than 1-chloropropane by a few per cents. Focusing on the four extreme state points explored in the simulation: 293.15 K – 0.1 MPa, 293.15 K – 200 MPa, 373.15 K – 0.1 MPa and 373.15 K – 200 MPa, the extrapolation of experimental densities of this work through a polynomial fitting of order 6 gives 'experimental' values of the density at these four states, respectively: 890.7, 1024.2, 783.7 and 965.9 kg·m^{-3} for 1-chloropropane and 864.7, 1001.6, 758.5 and 952.1 kg·m^{-3} for 2-chloropropane, respectively 2,9,

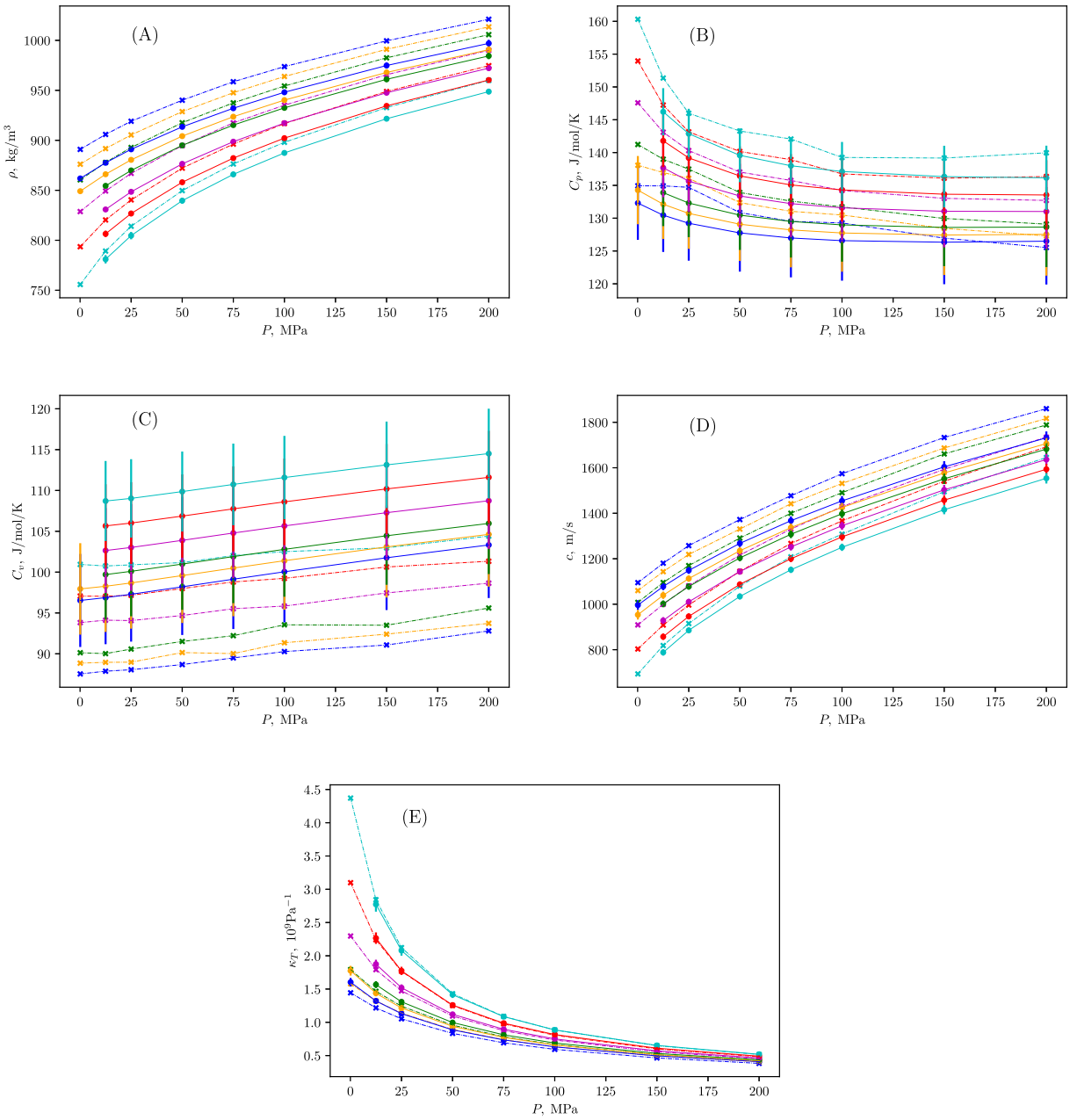

Fig. 5. The comparison of the values of density (A), heat capacity at constant pressure (B), heat capacity at constant volume (C), speed of sound (D) and isothermal compressibility (E) of 2-chloropropane, found from the MD simulation data (crosses) and by the obtained Span–Wagner EoS (circles) at the points where the simulations were made. Lines connect markers for visual guidance.

Table 2
The AADs for the thermodynamic properties of 1-chloropropane and 2-chloropropane from the MD simulations and Span–Wagner EoS.

AADs	1-chloropropane	2-chloropropane
ρ/%	0.543	2.141
C_P/%	3.415	2.407
C_V/%	4.734	9.128
c/%	3.820	26.928
κ_T/%	4.206	3.661

2.2, 3.2 and 1.4 % lower than for 1-chloropropane. The OPLS/ESP-HF/6-31G* model we have used gives densities for both liquids 1-chloropropane/2-chloropropane equal to 890/891, 1019/1021, 758/756, 988/960 kg·m^{-3} in the four states, respectively. Let us remind that in this work, the simulations of 1-chloropropane and 2-chloropropane are performed with rigid molecules.

In order to model the volume-dependent thermophysical properties accurately, it is crucial to get a very accurate reproduction of the density as a function of temperature and pressure. To see the effect of the force field, we did a *NPT* simulation with the AMBER package (release 18) and the GAFF2 force field [48,49] coupled to our set of charges of both liquids in the four previous states. After thermalization, with 150 ps runs, we got densities for both liquids 1-chloropropane/2-chloropropane equal to 885/883, 1006/1005, 765/763, 947/947 kg·m^{-3}. Doing the simulation with the same GAFF2 potential and our set of charges using the Lammps package [50] (the Oct. 2020 version), the densities were found to be equal to 862/859, 997/995, 717/718, 937/937 kg·m^{-3}, the error bars being around ±5 kg·m^{-3} except for the third state where it is around

± 10 kg·m^{-3}. The differences are due to differences in algorithmic features used in both packages. These tests also differ from our simulations because they fully include molecular flexibility.

Additionally, we performed another test to examine the effect of a charge model. We fitted a new set of ESP charges but we chose the grid points differently. The points where the electrostatic potential is computed are restrained with distances from atoms ranging from 1.00 to 1.01 times an atom's van der Waals radius. The simulation with the GAFF2 potential and the new charges using the Lammps package give densities equal to 858/859, 997/995, 722/711, 936/935 kg·m^{-3}. The effect of the set of the set of charges is thus very small, which is not unexpected because the electrostatic interaction energy is a small fraction of the cohesive energy for these liquids. The interesting information we get from these comparisons is that whatever the model one uses, the densities of both 1-chloropropane and 2-chloropropane remain very close at any thermodynamic state. Thus such models cannot be good for both liquids simultaneously. It thus seems that to improve the interaction model significantly, it will be necessary to modify the functional form and/or reconsider the transferability of parameters between both isomers. This task is a challenge for molecular modeling far beyond the scope of the present work.

6. Conclusions

In this work, we modeled the thermophysical properties of 1-chloropropane, 2-chloropropane, and 1,3-dichloropropane as a function of temperature and pressure using thermodynamic and molecular dynamics modeling. The study was motivated by the fact that halogenated propanes represent the most straightforward systems, which makes it possible to explore the effect on the thermodynamic properties of the liquid caused by the changes in molecular symmetry originating from the replacement of hydrogen by a heavy atom. Therefore, the study requires (i) the building of a high-accurate equation of state, which would be valid for a wide range of states. It would be based on a comprehensive critical evaluation of the existing experimental data and (ii) direct molecular dynamics simulations whose purpose is to test the conventional MD force fields. The differences associated with the various positions of a halogen atom allow us to capture the respective specificity of thermodynamic functions.

Thus, the main results can be formulated as follows:

1. we have found parameters for the Span–Wagner Equation of State, which has recently been considered the most accurate empiric multiparametric EoS (implemented in particular in the REFPROP system providing the standard reference data by the National Institute of Standard and Technologies), for all studied substances;
2. while building the model mentioned above, we critically evaluated the complete set of experimental data existing in the literature. We noted these data, which demonstrably deviate from the self-consistent thermodynamic model. We, therefore, proposed appropriate corrections that included their tabular form;
3. we explored the behavior of the thermal expansion coefficients in detail. Indeed, the IUPAC recommended this as a sensitive criterion for testing the accuracy of equations of state and was noted earlier as an open problem exhibiting a big difference between the compressed states of 1-chloropropane and 2-chloropropane. It is of specific fundamental interest to discuss the universality of its zero temperature isobaric derivative respective to the molecular packing and thermodynamic curvature;
4. in addition to this thermodynamic consideration, we reported and analyzed the results of the molecular dynamics simulations, which indicated the validity ranges of conventional force fields for reproducing the thermodynamics of 1-chloropropane and 2-chloropropane and posed required directions for future studies outside of these ranges.

Author Contributions

The manuscript was written through contributions of all authors. All authors have given approval to the final version of the manuscript.

Declaration of Competing Interest

The authors declare that they have no known competing financial interests or personal relationships that could have appeared to influence the work reported in this paper.

Acknowledgements

We are grateful for the financial support based on Decision No. 2016/23/B/ST8/02968 from the National Science Centre (Poland). We are grateful to the University of Silesia in Katowice, the Kursk State University, the University of Lorraine, the EXPLOR mesocentre and the CNRS for their support. PFM and CM thank Kanika Anand and Gérald Monard for their help in using the Lammps

References

[1] L. Xie, J. Zan, Z. Yang, Q. Wu, X. Chen, X. Ou, C. Lin, Q. Chen, H. Yang, A perovskite-based paper microfluidic sensor for haloalkane assays, Front. Chem. 9 (2021) 236, https://doi.org/10.3389/fchem.2021.682006.
[2] B. Li, L. Cui, C. Li, Macrocycle co-crystals showing vapochromism to haloalkanes, Angew. Chem. Int. Ed. 59 (49) (2020) 22012–22016, https://doi.org/10.1002/anie.202010802.
[3] X. Wang, E. Wright, N. Gao, Y. Li, Evaluation on excess entropy scaling method predicting thermal transport properties of liquid hfc/hfo refrigerants, J. Therm. Sci. (2020) 1–11, https://doi.org/10.1007/s11630-020-1383-2.
[4] I. Polishuk, M. Katz, Y. Levi, H. Lubarsky, Implementation of pc-saft and saft+ cubic for modeling thermodynamic properties of haloalkanes. i. 11 halomethanes, Fluid Ph. Equilibria 316 (2012) 66–73, https://doi.org/10.1016/j.fluid.2011.12.003.
[5] U.K. Deiters, K.M. De Reuck, Guidelines for publication of equations of state I. Pure fluids (Technical Report), Pure Appl. Chem. 69 (1997) 1237–1250.
[6] S.L. Randzio, J.-P. Grolier, M. Chorążewski, High-Pressure 'Maxwell Relations' Measurements, The Royal Chemical Society, London, 2015, pp. 414–438.
[7] M. Taravillo, V.G. Baonza, M. Cáceres, J. Núñez, Thermodynamic regularities in compressed liquids: I. the thermal expansion coefficient, J. Phys.: Condens. Matter 15 (19) (2003) 2979, https://doi.org/10.1088/0953-8984/15/19/302.
[8] P. Navia, J. Troncoso, L. Romaní, Isobaric thermal expansivity for nonpolar compounds, J. Chem. Eng. Data 55 (6) (2010) 2173–2179, https://doi.org/10.1021/je900757k.
[9] H. Guerrero, L.M. Ballesteros, M. García-Mardones, C. Lafuente, I. Gascón, Volumetric properties of short-chain chloroalkanes, J. Chem. Eng. Data 57 (2012) 2076–2083, https://doi.org/10.1021/je3003805.
[10] M. Chorążewski, J. Troncoso, J. Jacquemin, Thermodynamic properties of dichloromethane, bromochloromethane, and dibromomethane under elevated pressure: Experimental results and saft-vr mie predictions, Ind. Eng. Chem. Res. 54 (2) (2015) 720–730, https://doi.org/10.1021/ie5038903.
[11] V.V. Melent'ev, E.B. Postnikov, Speed of sound and density of 1-chloropropane in the range of temperatures 180–373 K and pressures up to 196.1 MPa, J. Chem. Eng. Data 62 (2017) 3409–3413, https://doi.org/10.1021/acs.jced.7b00443.
[12] M. Frenkel, R.D. Chirico, V. Diky, X. Yan, Q. Dong, C. Muzny, ThermoData Engine (TDE): software implementation of the dynamic data evaluation concept, J. Chem. Inf. Model. 45 (2005) 816–838, https://doi.org/10.1021/ci050067b.
[13] V. Diky, C.D. Muzny, E.W. Lemmon, R.D. Chirico, M. Frenkel, ThermoData Engine (TDE): Software implementation of the dynamic data evaluation concept. 2. Equations of state on demand and dynamic updates over the web, J. Chem. Inf. Model. 47 (2007) 1713–1725, https://doi.org/10.1021/ci700071t.

[14] A.R. Lowe, B. Jasiok, V.V. Melent'ev, O.S. Ryshkova, V.I. Korotkovskii, A.K. Radchenko, E.B. Postnikov, M. Spinnler, U. Ashurova, J. Safarov, E. Hassel, M. Chorążewski, High-temperature and high-pressure thermophysical property measurements and thermodynamic modelling of an international oil standard: RAVENOL diesel rail injector calibration fluid, Fuel Process. Technol. 199 (2020) 106220, https://doi.org/10.1016/j.fuproc.2019.106220.
[15] W.M. Rutherford, Viscosity and density of some lower alkyl chlorides and bromides, J. Chem. Eng. Data 33 (1988) 234–237, https://doi.org/10.1021/je00053a003.
[16] V.V. Melent'ev, E.B. Postnikov, Density and speed of sound of 2-chloropropane in the range of temperatures 293.15–373.15 K and pressures up to 196.2 MPa, Chem. Data Collect. 24 (2019) 100270, https://doi.org/10.1016/j.cdc.2019.100270.
[17] V.V. Melent'ev, E.B. Postnikov, Influence of isomerization on acoustic and fluctuation properties of chloropropanes according to experimental and model studies, in: Proceedings of the XXXII Session of the Russian Acoustical Society, Moscow, Octover 14–18, 2019, GEOS (Moscow), 2019, pp. 1245–1250. URL: http://rao.akin.ru/images/32%20isbn.zip.
[18] M. Chorążewski, A. Grzybowski, M. Paluch, The complex, non-monotonic thermal response of the volumetric space of simple liquids, Phys. Chem. Chem. Phys. 16 (2014) 19900–19908, https://doi.org/10.1039/C4CP02350A.
[19] ThermoData Engine (TDE)Version 10: NIST standard reference database 103b (2015).
[20] F. Yebra, K. Zemánková, J. Troncoso, Speed of sound as a function of temperature and pressure for propane derivatives, J. Chem. Thermodyn. 109 (2017) 117–123, https://doi.org/10.1016/j.jct.2016.12.016.
[21] Y. Meléndez-Pagaán, B.E. Taylor, D. Ben-Amotz, Cavity formation and dipolar contribution to the gauche-trans isomerization of 1-chloropropane and 1,2-dichloroethane, J. Phys. Chem. B 105 (2001) 520–5262, https://doi.org/10.1021/jp002781w.
[22] A. Bondi, Van der waals volumes and radii, J. Phys. Chem. 68 (1964) 441–451.
[23] R.S. Rowland, R. Taylor, Intermolecular nonbonded contact distances in organic crystal structures: Comparison with distances expected from van der waals radii, J. Phys. Chem. 100 (1996) 7384–7391, https://doi.org/10.1021/jp953141+.
[24] M.J. Frisch, G.W. Trucks, H.B. Schlegel, G.E. Scuseria, M.A. Robb, J.R. Cheeseman, G. Scalmani, V. Barone, B. Mennucci, G.A. Petersson, H. Nakatsuji, M. Caricato, X. Li, H.P. Hratchian, A.F. Izmaylov, J. Bloino, G. Zheng, J.L. Sonnenberg, M. Hada, M. Ehara, K. Toyota, R. Fukuda, J. Hasegawa, M. Ishida, T. Nakajima, Y. Honda, O. Kitao, H. Nakai, K. Vreven, J.A. Montgomery, Jr., J.E. Peralta, F. Ogliaro, M. Bearpark, J.J. Heyd, E. Brothers, K.N. Kudin, V.N. Staroverov, T. Keith, R. Kobayashi, J. Normand, K. Raghavachari, A. Rendell, J.C. Burant, S.S. Iyengar, J. Tomasi, M. Cossi, N. Rega, J.M. Millam, M. Klene, J.E. Knox, J.B. Cross, V. Bakken, C. Adamo, J. Jaramillo, R. Gomperts, R.E. Stratmann, O. Yazyev, A.J. Austin, R. Cammi, C. Pomelli, J.W. Ochterski, R.L. Martin, K. Morokuma, V.G. Zakrzewski, G.A. Voth, P. Salvador, J.J. Dannenberg, S. Dapprich, A.D. Daniels, O. Farkas, J.B. Foresman, J.V. Ortiz, J. Cioslowski, D.J. Fox, Gaussian 09,Revision D.01, Gaussian Inc., Wallingford CT (2013).
[25] W.L. Jorgensen, D.S. Maxwell, J. Tirado-Rives, Development and testing of the opls all-atom force field on conformational energetics and properties of organic liquids, J. Am. Chem. Soc. 118 (1996) 11225–11236, https://doi.org/10.1021/ja9621760.
[26] M. Svanberg, An improved leap-frog rotational algorithm, Mol. Phys. 92 (1997) 1085–1088, https://doi.org/10.1080/002689797169727.
[27] D. Fincham, Leapfrog rotational algorithm, Mol. Simul. 24 (1992) 33–69, https://doi.org/10.1080/08927029208022474.
[28] M.P. Allen, D.J. Tildesley, Computer Simulation of Liquids, Oxford University Press, Oxford, 1987.
[29] A.J.C. Ladd, Monte carlo simulation of water, Mol. Phys. 33 (1977) 1039–1050, https://doi.org/10.1080/00268977700100921.
[30] A.J.C. Ladd, Long-range dipolar interactions in computer simulations of polar liquids, Mol. Phys. 36 (1978) 463–474, https://doi.org/10.1080/00268977800101701.
[31] M. Neumann, Dielectric properties and the convergence of multipolar lattice sums, Mol. Phys. 60 (1987) 225–235, https://doi.org/10.1080/00268978700100171.
[32] C. Millot, J.-L. Rivail, R. Diguet, Static dielectric constant density and temperature dependence for the tips model of liquid methyl chloride, Chem. Phys. Lett. 160 (1989) 228–232, https://doi.org/10.1016/0009-2614(89)87587-6.
[33] F. Dehez, M.T.C. Martins Costa, D. Rinaldi, C. Millot, Long-range electrostatic interactions in hybrid quantum and molecular mechanical dynamics using a lattice summation approach, J. Chem. Phys. 122 (2005) 234503, https://doi.org/10.1063/1.1931667.
[34] D.J. Adams, G.S. Dubey, Taming the ewald sum in the computer simulation of charged systems, J. Comput. Phys. 72 (1987) 156–176, https://doi.org/10.1016/0021-9991(87)90076-3.
[35] B. Cichocki, B.U. Felderhof, K. Hinsen, Electrostatic interactions in periodic coulomb and dipolar systems, Phys. Rev. A 39 (1989) 5350–5358, https://doi.org/10.1103/PhysRevA.39.5350.
[36] C. Millot, J.-C. Soetens, M.T.C. Martins Costa, Static dielectric constant of the polarizable stockmayer fluid. comparison of the lattice summation and reaction field methods, Mol. Simul. 18 (1997) 367–383, https://doi.org/10.1080/08927029708024131.
[37] K. Shimaoka, M. Kinoshita, K. Fujii, T. Tosaka, valuation of measurement data-supplement 1 to the guide to expression of uncertainty in measurement-propagation of distributions using a monte carlo method, https://www.bipm.org/documents/20126/2071204/JCGM_101_2008_E.pdf/325dcaad-c15a-407c-1105-8b7f322d651c, [Online; accessed 16-November-2021] (2008).
[38] K. Shimaoka, M. Kinoshita, K. Fujii, T. Tosaka, Evaluation of measurement data—guide to the expression of uncertainty in measurement, https://www.bipm.org/documents/20126/2071204/JCGM_100_2008_E.pdf/cb0ef43f-baa5-11cf-3f85-4dcd86f77bd6, [Online; accessed 16-November-2021] (2008).
[39] P.W. Bridgman, The Pressure-Volume-Temperature Relations of Fifteen Liquids, Proc. Am. Acad. Arts Sci. 68 (1933) 1–25, https://doi.org/10.2307/20022928.
[40] A.A. Pribylov, E.B. Postnikov, Thermodynamic curvature and the thermal expansion isolines, J. Mol. Liq. 335 (2021) 115994, https://doi.org/10.1016/j.molliq.2021.115994.
[41] M.F. Bolotnikov, Y.A. Neruchev, The enthalpies of vaporization and intermolecular interaction energies of 1-chloroalkanes, Russ. J. Phys. Chem. 80 (2006) 1191–1197, https://doi.org/10.1134/S0036024406080024.
[42] V.V. Melent'ev, E.B. Postnikov, I. Polishuk, Experimental determination and modeling thermophysical properties of 1-chlorononane in a wide range of conditions: is it possible to predict a contribution of chlorine atom?, Ind Eng. Chem. Res. 57 (2018) 5142–5150, https://doi.org/10.1021/acs.iecr.8b00174.
[43] J.-L. Daridon, D. Nasri, J.-P. Bazile, Computation of isobaric thermal expansivity from liquid density measurements application to toluene, J. Chem. Eng. Data 12 (2021), https://doi.org/10.1021/acs.jced.1c00634.
[44] J.L. Lebowitz, J.K. Percus, L. Verlet, Ensemble dependence of fluctuations with application to machine computations, Phys. Rev. 153 (1967) 250–254, https://doi.org/10.1103/PhysRev.153.250.
[45] P.S.Y. Cheung, On the calculation of specific heats, thermal pressure coefficients and compressibilities in molecular dynamics simulations, Mol. Phys. 33 (1977) 519–526, https://doi.org/10.1080/00268977700100441.
[46] J.R. Durig, X. Zhu, S. Shen, Conformational and structural studies of 1-chloropropane and 1-bromopropane from temperature-dependant ft-ir spectra of rare gas solutions and ab initio calculations, J. Mol. Struct. 570 (2001) 1–23, https://doi.org/10.1016/S0022-2860(01)00473-2.
[47] P. Klaboe, The vibrational spectra of 2-chloro, 2-bromo, 2-iodo and 2-cyanopropane, Spectrochim. Acta 26A (1970) 87–108, https://doi.org/10.1016/0584-8539(70)80253-7.
[48] D.A. Case, T.E. Cheatham III, T. Darden, H. Gohlke, R. Luo, K.M. Merz Jr., A. Onufriev, C. Simmerling, B. Wang, R.J. Woods, The amber biomolecular simulation programs, J. Comput. Chem. 26 (2005) 1668–1688, https://doi.org/10.1002/jcc.20290.
[49] R. Salomon-Ferrer, D.A. Case, R.C. Walker, An overview of the amber biomolecular simulation package, WIREs Comput. Mol. Sci. 3 (2013) 198–210, https://doi.org/10.1002/wcms.1121.
[50] A.P. Thompson, H.M. Aktulga, R. Berger, D.S. Bolintineanu, W.M. Brown, P.S. Crozier, P.J. in 't Veld, A. Kohlmeyer, S.G. Moore, T.D. Nguyen, R. Shan, M.J. Stevens, J. Tranchida, C. Trott, S.J. Plimpton, Lammps - a flexible simulation tool for particle-based materials modeling at the atomic, meso, and continuum scales, Comput. Phys. Commun. 271 (2022) 108171, https://doi.org/10.1016/j.cpc.2021.108171.